ACS OMEGA

Open Access

http://pubs.acs.org/journal/acsodf

Article

Molecular Insights into the Binding of Organophosphate Flame Retardant Key Metabolites with Mineralocorticoid and Estrogen Receptors

Syeda Sumayya Tariq,[#] Madiha Sardar,[#] Muhammad Shafiq, Muhammad Huzaifa, Mohammad Nur-e-Alam, Yan Wang, and Zaheer Ul-Haq*

Cite This: *ACS Omega* 2025, 10, 20015−20025

Read Online

ACCESS | Metrics & More | Article Recommendations | Supporting Information

ABSTRACT: Flame retardants (FR) encompass a wide range of chemicals designed to inhibit and reduce the spread of fire by forming protective layers on materials. While originally considered relatively safe due to their rapid metabolism, growing evidence indicates that organophosphate flame retardants (OPFRs) can be extensively released into the environment, leading to toxic effects in humans, particularly endocrine disruption. Although the endocrine-disrupting potential of OPFRs is well-documented, the mechanisms through which their metabolites exert toxic effects remain largely unexplored. In this study, a comprehensive computational framework incorporating molecular docking, density functional theory, and all-atom molecular dynamic simulations were employed to investigate the binding and interactions of three key OPFR metabolites, BCIPP, BDCIPP, and DPHP, with human estrogen receptors (ER) and mineralocorticoid receptors (MR). The results revealed that these metabolites formed stable and compact complexes with both MR and ER, although high per residue atomic fluctuations were observed in ER complexes, likely due to the reactive nature of the metabolites. Binding free energy analysis further indicated favorable interactions between the OPFR metabolites and target receptors. Principal component analysis, leveraging machine learning algorithms, showed consistent motion, while free energy profiles demonstrated stable energy basins with minimal variations. These findings suggest that OPFR metabolites have strong binding affinities with MR and ER, hinting at their potential endocrine-disrupting effects at the molecular level. This study lays the groundwork for future research into the hazards posed by OPFR metabolites.

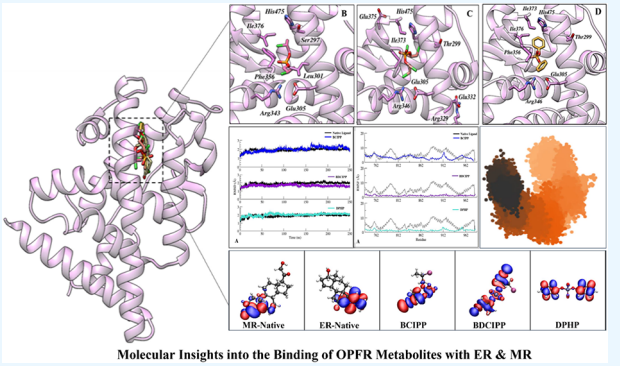

Molecular Insights into the Binding of OPFR Metabolites with ER & MR

1. INTRODUCTION

Flame retardants (FRs) encompass a wide array of chemicals designed to inhibit the ignition of materials or significantly slow the spread of fire by creating a protective layer over the products.[1] FRs are widely used across various industries, commonly incorporated into products such as plastics, furniture, textiles, paint, circuit boards, and building materials to enhance fire safety.[2−4] The term describes their functional purpose rather than their specific chemical composition.[5] After the restrictions imposed on halogenated FR, organophosphate flame retardants (OPFRs) are increasingly being used as alternatives.[6] Although initially considered relatively safe due to their high rate of metabolism, evidence now indicates that OPFRs can be extensively released into the environment. This results in exposure primarily through inhalation or ingestion of household dust and dermal absorption from contact with furniture and fabrics and via breast milk in infants.[7] These exposures are linked to toxic effects in humans, including carcinogenicity, endocrine disruption, and neurotoxicity.[8,9]

OPFRs, derived from phosphoric acid, consist of either straight (alkyl) or ring-shaped (cycloalkyl) chains. Examples include tris(1-chloro-2-propyl) phosphate (TCIPP), triphenyl phosphate (TPHP), and tris(1,3-dichloro-2-propyl) phosphate (TDCIPP), which are efficiently metabolized by cytochrome P450 (CYP) enzymes in liver microsomes. These findings are corroborated by research that has identified various FR metabolites in urine samples, including dibutyl phosphate (DBP), bis(2-chloroethyl) phosphate (BCEP), bis(1-chloro2-propyl) phosphate (BCIPP), bis(1,3-dichloro-2-propyl) phosphate (BDCIPP), and diphenyl phosphate (DPHP). Among

Received: March 5, 2025
Accepted: April 25, 2025
Published: May 7, 2025

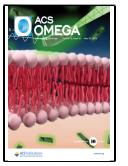

these metabolites, BDCIPP, DPHP, and BCIPP were found in high concentrations, particularly prominent in adult urine.[10,11]

Health risk assessments for OPFRs are primarily focused on their potential to disrupt the endocrine system. Several studies have established that different OPFRs exhibit steroid hormone mimicry by interacting with estrogen receptors (ER), mineralocorticoid receptor (MR), and androgen receptors (AR), disrupting hormone synthesis, and induction of reproductive defects.[12,13] In-vitro and in vivo studies have also suggested that the three specific OPFR metabolites, BDCIPP, DPHP, and BCIPP, exhibit agonistic activity toward the rat ER, conversely, these metabolites display antagonistic activity toward the human mineralocorticoid MR.[14] Furthermore, epidemiological studies suggest a progressive link between the potential estrogenic activity of OPFRs and increased prolactin levels, as well as a decrease in sperm quality.[15] Despite evidence of endocrine disruption by the parent OPFRs and the potential for similar disruption by their main primary metabolites, BCIPP, BDCIPP, and DPHP, the underlying mechanisms by which these metabolites exert their toxic effects remain largely unexplored.

In this context, the study aims to identify the binding interaction patterns of the three primary OPFR metabolites and to explore their atomic-level effects on human ER and MR. A multifaceted computational framework was employed, involving in silico techniques such as molecular docking to explore binding sites and density functional theory (DFT) techniques to calculate electrostatic potential and reactivity descriptors. Additionally, an all-atom molecular dynamics (MD) simulation was used to assess stability by examining deviation patterns, local flexibility shifts, and time-dependent gyration profiles as well as calculating free binding energies.

To gain a deeper understanding of the dynamics and interactions within protein−ligand complexes, principal component analysis (PCA) was conducted in order to simplify and highlight essential features of the complex data sets produced by MD simulations. Subsequently, free energy landscapes (FELs) were employed to reveal conformational changes associated with different energy states and thermodynamic variations in the protein structure. This comprehensive analysis aims to provide a deep understanding of the molecular interactions between OPFR metabolites and receptors, serving as a foundation for future investigations of the potential hazards of OPFR metabolites.

2. METHODOLOGY

2.1. Ligand Preparation. The three primary OPFR metabolites, BCIPP, BDCIPP, and DPHP, were chosen for the current study leveraging on the experimental validation of their endocrine disruption activity.[14] The chemical structures of these compounds, as identified in Table 1, were generated by using ChemDraw software. The MMFF94 force field included in the Molecular Operating Environment (MOE) package was used to supply hydrogen, minimize energy, and apply partial charges to these compounds.[16,17] Prior to charge fitting, energy minimization was performed on each compound by using the default RMS gradient of 0.1 kcal/mol/Å^2. These preliminary actions were performed in order to derive spatial coordinates for each molecule that correspond to the most energetically favorable configuration. Subsequent docking studies used the optimized molecules as input files.

2.2. Protein Preparation. This study is focused on two key proteins: The MR and the ER. The structures of these proteins, retrieved from the Protein Data Bank with the PDB IDs 1Y9R[18] and 4J26,[19] respectively, serve as the preliminary point for further analysis. In the course of the protein preparation phase, several modifications were made to the structures, such as adding missing atoms and residues, adjusting bond orders, and formal charges. The protonate 3D algorithm was used to incorporate hydrogen atoms.[20] For protonation, the electrostatic function employed the generalized Born volume integral (GB/VI) method with a solvent dielectric value of 80. van der Waals and electrostatic cutoffs were set at 10 and 15 Å, respectively.[21] The MOE software suite's AMBER99 force field was used to apply partial charges.

Table 1. OPFR Metabolites—Bis(1-chloro2-propyl) Phosphate (BCIPP), Bis(1,3-dichloro-2-propyl) Phosphate (BDCIPP), and Diphenyl Phosphate (DPHP)

S. No.	Compounds	Structure
1	BCIPP	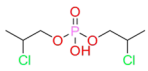
2	BDCIPP	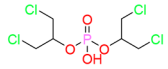
3	DPHP	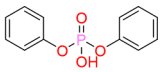
4	Estradiol (Native Ligand – ER)	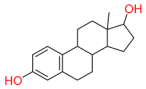
5	Desoxycorticosterone (Native Ligand – MR)	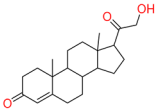

2.3. Molecular Docking. The 3D structures of both the MR and ER were loaded into the MOE-dock interface for the docking simulations. Before the docking studies were conducted, the docking software was benchmarked by comparing the root-mean-square deviation (RMSD) values between the crystal structure coordinates of the native ligands of both the proteins and the simulated pose. This evaluation, aimed at reproducing known binding geometries, validated the chosen docking protocol for further studies. The docking simulations employed the Triangle Matcher algorithm for placement and the London dG scoring function with an Induced Fit approach for each protein. Afterward, ten conformations were generated for each studied OPFR metabolite while maintaining all other parameters at their default settings. The ligand conformation with the lowest docking score, signifying the strongest binding affinity, was chosen for further analysis of its binding orientation and interaction profile with both the ER and MR.

2.4. DFT. All-electron DFT calculations were performed with the CP2K code using triple-ζ quality 6-311G(d,p) pople-style basis set[22,23] and B3LYP exchange−correlation functional.[24,25] The energy cutoff was set to 450 Ry, which is sufficient for the convergence of the self-consistent field (SCF) cycle. All of the ligands were allowed to relax until the maximum force in a molecule reached below 0.01 eV/atom Å. Vibrational analysis was conducted to validate the optimized

https://doi.org/10.1021/acsomega.5c02044
ACS Omega 2025, 10, 20015−20025

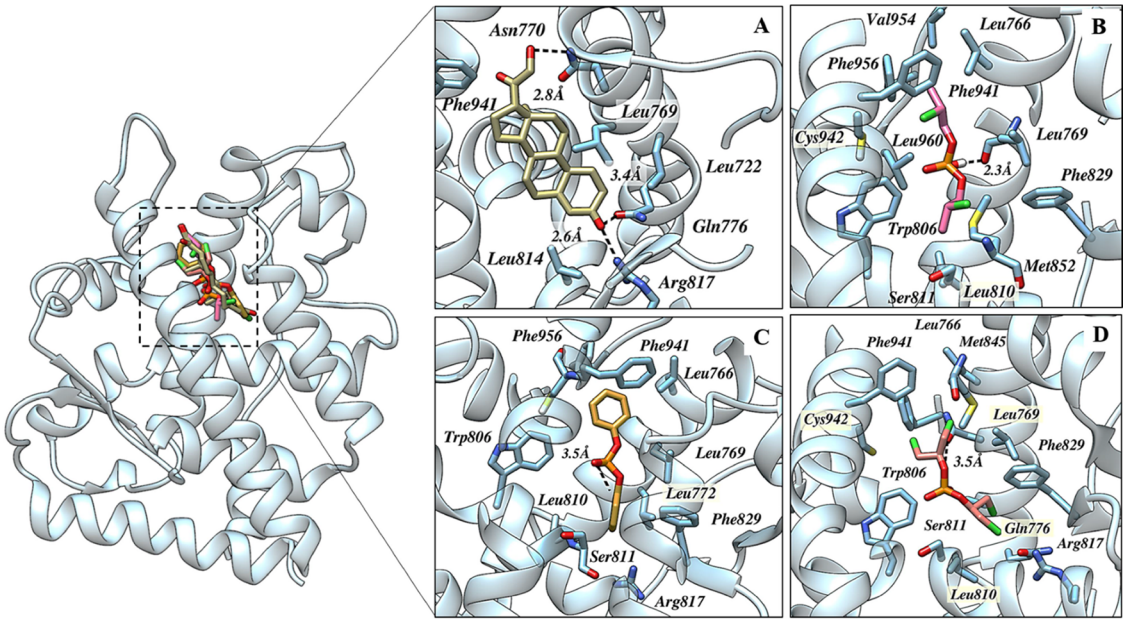

Figure 1. Binding orientation of MR in complex with (A) Native Ligand, (B) BCIPP, (C) DPHP, and (D) BDCIPP. The dashed black line represents hydrogen bonding. Pictures were rendered using UCSF Chimera.

structures, and all structures showed real vibrational frequencies, thus validating the trueness of optimized geometries.

2.5. All-Atom MD Simulation. A comprehensive all-atom MD simulation of ER and MR in complex with BCIPP, BDCIPP, DPHP, and their native ligands, desoxycorticosterone, and estradiol, respectively, was carried out using the PMEMD algorithm with the CUDA acceleration module integrated into Amber22.[26] The topologies for target protein complexes were created using the antechamber and tleap modules.[27] The eight systems were immersed in a solvent environment generated with TIP3P, an explicit water model, inside a periodic box with atoms of the protein separated by at least 10 Å.[28] The steepest descent approach with 2500 steps was used to minimize energy and conjugate gradients in the systems.[29] Position constraints were used to hold the protein in place, and the process was repeated six times, each time progressively decreasing the degree of restraint. After the last restriction was lifted, the systems proceeded through another round of energy minimization. To achieve the target temperature of 300 K, the systems were heated for 500 ps under a continuous volume-temperature (*NVT*) ensemble. The process was repeated twice, gradually reducing the positional limitations from 30 to 10 kcal mol. The system was equilibrated by using a two-phase process: first under constant pressure (*NPT*) and then under constant volume (*NVT*). The *NPT* equilibration was performed in three steps over a total of 1.5 ns with the temperature gradually increased to 300 K. This temperature increase was carried out in a controlled manner to ensure smooth thermal stabilization. Following this, *NVT* equilibration was performed in seven steps over 4.5 ns, with the restraint weights gradually reduced in each step to allow the system to adapt to its natural dynamics. The final step of this phase was performed without any restraints, allowing the system to equilibrate freely at 300 K and 1 atm. Throughout the entire equilibration process, the system's stability was closely monitored by tracking the convergence of key properties, such as temperature and pressure. The system was considered equilibrated when both the temperature and pressure exhibited stable oscillating behavior within desired thresholds, indicating that optimal conditions for production runs had been achieved. Ultimately, eight complexes in total, a production run of 250 ns (2 μs) each, were executed under periodic boundary conditions. With the use of Langevin dynamics and isotropic position scaling, the temperature and pressure were controlled. The Particle Mesh Ewald (PME) approach was used to investigate long-range electrostatic interactions.[30] The SHAKE algorithm was employed to limit the interactions involving H atoms, and the nonbonded interactions were identified by using a cutoff of 10 Å.[31] The numerical integration was set up in two femtosecond time steps. The simulated trajectories were examined using Chimaera, VMD, and the CPPTRAJ modules.[32−34] As stability measurements, RMSD, root-mean-square fluctuation (RMSF), and radius of gyration (R_g) were considered.

2.6. Binding Free Energy. Free energy of binding was calculated by the Molecular Mechanics-Generalized Born (MM-GBSA) approach, where the last 50 ns trajectories (25 frames per nanosecond) were used to perform calculations through the MMPBSA.py tools in the AMBER 22 package.[35] Mathematically, the value of (ΔG_{bind}) was determined using eq 1, which takes into account the contributions of free energy in the gas term (eq 2), free energy in the solvation term (eq 3), and changes in entropy. The energy in the gas term (ΔG_{gas}) comprises electrostatic energy (ΔG_{ele}) and van der Waals energy (ΔG_{vdW}). The energy contribution to the solvation term (ΔG_{solv}) is composed of the polar solvation energy (ΔG_{solv}^{ele}) and the energy associated with the solvent-accessible surface area ($\Delta G_{solv}^{nonpolar}$).[36]

$$\Delta G_{bind} = \Delta G_{gas} + \Delta G_{solv} - T\Delta S \quad (1)$$

$$\Delta G_{gas} = \Delta G_{vdW} + \Delta G_{ele} \quad (2)$$

$$\Delta G_{solv} = \Delta G_{solv}^{ele} + \Delta G_{solv}^{nonpolar} \quad (3)$$

https://doi.org/10.1021/acsomega.5c02044
ACS Omega 2025, 10, 20015−20025

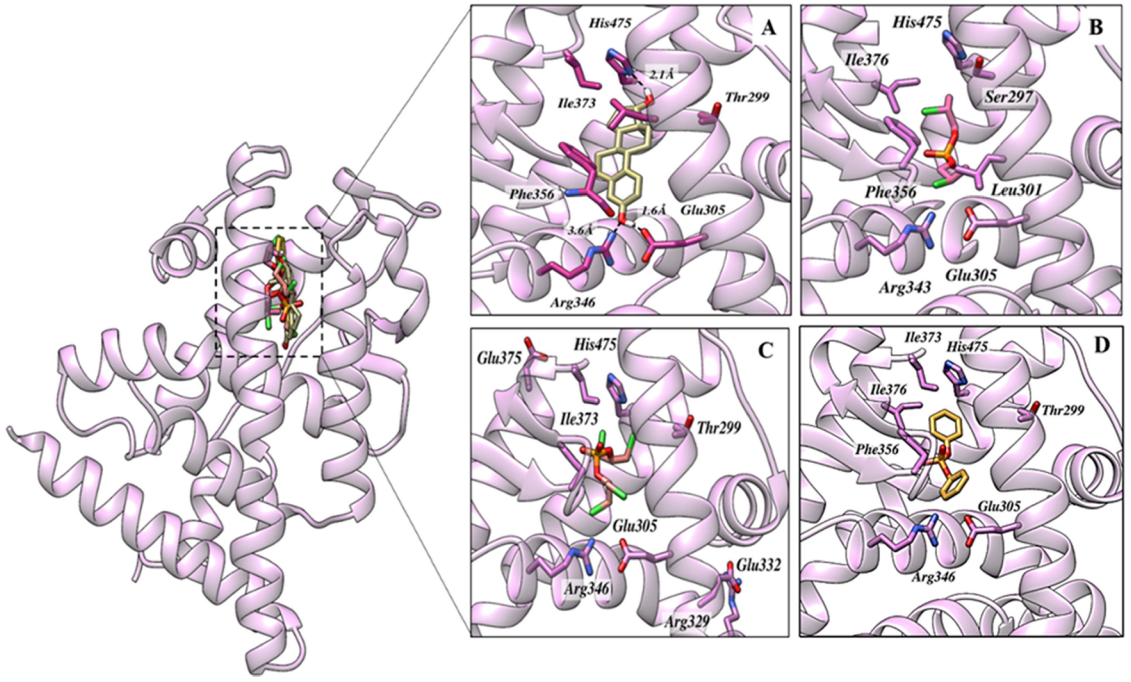

Figure 2. Binding orientation of ER in complex with (A) Native Ligand, (B) BCIPP, (C) BDCIPP, and (D) DPHP. The dashed black line represents hydrogen bonding. Pictures were rendered utilizing UCSF Chimera.

2.7. PCA. PCA was used to simplify the complex data from MD simulation in order to reduce its dimensions and reveal important patterns and relationships within the dataset. Its objective also included examining conformational changes in proteins and deriving significant conclusions from the complex movements seen in MD trajectories. PCA was firmly grounded by aligning the MD trajectories with the default parameters. By diagonalizing the matrix, the Essential Dynamics (ED) approach was used to calculate the eigenvectors, eigenvalues, and their projections. The PCA module of the MDAnalysis tools was used to do the analysis, utilizing the two main components.[37] In addition, the simulated system's free energy profile was created using the data from these primary components.

2.8. FEL. The FEL was constructed by using the gmx sham plugin of the GROMACS software package after the conformational landscape and the molecular motions examined by the simulations were evaluated. The following formula illustrates potential protein conformations during MD simulations with respect to Gibbs free energy based on the first two main components.[38]

$$\Delta G = -K_B T \ln P(PC_1, PC_2) \quad (4)$$

The probability distribution of the molecular system with its two primary components is represented by $P(PC_1, PC_2)$ in this equation, where K_B and T stand for the Boltzmann constant and absolute temperature, respectively. The energy distribution of the system is represented visually by the FEL, which offers a glimpse into the kinetics and thermodynamic stability of the molecules by exposing different energy states and the conformational probabilities that go along with them.

3. RESULTS AND DISCUSSION

3.1. Interaction Pattern Analysis of MR. Molecular docking was employed to investigate the binding of the OPFR metabolites with the MR to provide insight into their comprehensive binding modes and potential competition with the native ligands of the MR. In this context, structural coordinates of the MR were used as the foundational framework. The selection process was then based on a combination of favorable binding orientations and effective interactions with key residues.[39,40]

The native ligand exhibited a high binding affinity for the MR receptor owing to a network of critical interactions, including multiple hydrogen bonds established with the MR residues Asn770, Leu769, and Leu814, at distances of 2.8, 2.6, and 3.4 Å, respectively, while residues Leu722, Gln776, Arg817, and Phe941 were found involved in hydrophobic bonding, with a docking score of −10.49 kcal/mol (Figure 1A). In the case of BCIPP, several key residues were found to exhibit intermolecular interaction patterns, including Leu766, Leu769, Trp806, Leu810, Ser811, Phe829, Met852, Phe941, Cys942, Val954, and Phe956, while a hydrogen bond was established with the oxygen atom of carbonyl on Leu769 spanning a distance of 2.3 Å (Figure 1B) with a docking score of −7.13 kcal/mol. Among the studied compounds, DPHP exhibited the highest docking score, with a value of −7.28 kcal/mol. Analysis of its interactions within the binding pocket revealed that DPHP primarily forms favorable hydrophobic interactions with several key residues: Leu772, Leu766, Leu769, Trp806, Leu810, Ser811, Phe829, Met852, Phe941, Val954, and Phe956. These hydrophobic interactions likely contribute to stabilizing the DPHP-MR interactions as illustrated in (Figure 1C). In addition, $\pi-\pi$ stacking interactions were also observed involving the residues Phe829 and Phe941. In the case of BDCIPP, a hydrogen bond was established with the oxygen atom of the carbonyl group on Leu769 at a distance of 3.5 Å (Figure 1D). BDCIPP is primarily surrounded by a cluster of nonpolar residues, including Leu766, Trp806, Leu810, Ser811, Phe941, Cys942, Val954, and Phe956, which contribute to a favorable hydrophobic environment. The binding affinity was found to

https://doi.org/10.1021/acsomega.5c02044
ACS Omega 2025, 10, 20015−20025

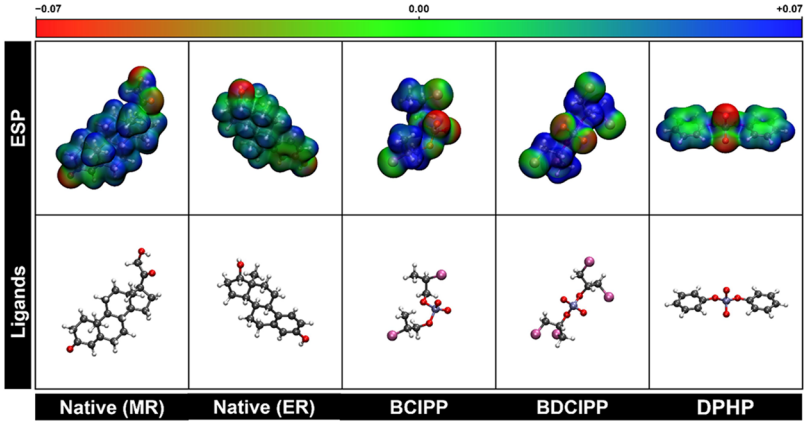

Figure 3. Optimized structures and ESP isosurfaces of the studied ligands. C, H, O, P, and Cl atoms are represented by gray, white, red, light blue, and light purple, respectively. Isovalue: 0.006*e*.

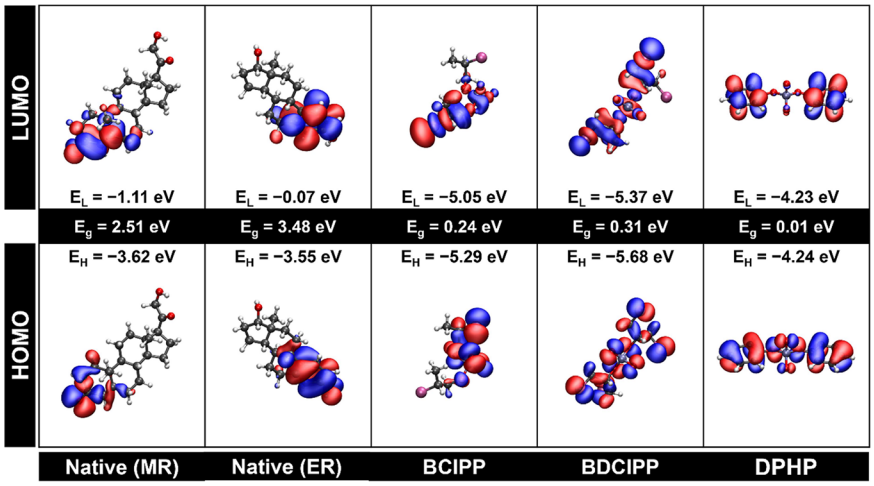

Figure 4. Frontier molecular orbitals of the studied ligands. Isovalue: 0.02*e*.

be −7.24 kcal/mol. Notably, some common residues were found taking part in hydrophobic interactions with the OPFR metabolites, including Leu772, Leu766, Leu769, Trp806, Leu810, Ser811, Phe829, Met852, Phe941, Val954, and Phe956, and can be considered to play a significant role in stabilizing the interactions of OPFR metabolites with MR.

3.2. Interaction Pattern Analysis of ER. Molecular docking was employed to investigate the interactions of OPFR metabolites with the ER to provide insight into their comprehensive binding modes and interaction patterns. Upon examination, the strong binding was noted for the OPFRs metabolites toward ER with the docking score ranging from −7.72 to −7.52 kcal/mol. The native ligand interacts with several key residues through hydrogen bonds, hydrophobic interactions, and van der Waals forces. The nitrogen atom of His475 formed a hydrogen bond with the hydroxyl group of native spanning a distance of 2.1Å. An additional hydrogen bond was formed with the carbonyl group of Glu305 with the hydroxyl group of the native ligand at a distance of 1.6 Å. On the other hand, the nitrogen atom of Arg346 established a hydrogen bond with the hydroxyl group of the native ligand spanning a distance of 3.6 Å, indicating strong interactions. The docking score was measured at −9.69 kcal/mol (Figure 2A). Analysis of BCIPP demonstrated the existence of a network of hydrophobic interactions involving residues Ser297, Leu301, Glu305, Arg343, Phe356, Ile376, and His475. These residues play a key role for the stability of BCIPP-MR interaction (Figure 2B). Similar to BCIPP, analysis of BDCIPP and DPHP exhibited multiple hydrophobic interactions involving residues Glu305, Arg343, Ile376, and His475 (Figure 2C,D). Additionally, BDCIPP exhibits novel interactions with other residues, Arg329 and Glu375, and potentially Glu332, offering the maximum interaction pattern toward ER, exhibiting the strongest binding affinity to ER among the metabolites. In addition, $\pi-\pi$ stacking interactions were also observed involving the residues Phe829 and Phe941. In vitro studies have demonstrated that BDCIPP, DPHP, and BCIPP exhibit agonistic activity toward the ER, suggesting their ability to mimic steroid hormones.[14] Residues Thr299, Leu301, Glu305, Arg343, Ile376, and His475 contribute to stabilizing the native ligand with ER through hydrophobic interactions, similar to those observed with the OPFR metabolites; therefore, these residues can be considered as crucial in stabilizing the interaction.

3.3. Electrostatic Potential (ESP) Map. The ESP map helps predict the electrophilic and nucleophilic attack sites in a molecule. The ground-state structures and ESP maps of the studied ligands are depicted in Figure 3. The red, blue, and green contours represent negative (electron-rich), positive (electron-deficient), and neutral regions, respectively. The red and blue regions also indicate favorable sites for electrophilic and nucleophilic attack. In both ER and MR, red and blue

https://doi.org/10.1021/acsomega.5c02044
ACS Omega 2025, 10, 20015−20025

Table 2. Reactivity Parameters for the Studied Ligands[a]

	ligand	EH	EL	E_g	IP	EA	χ	μ	H	ω
1	native (MR)	−3.62	−1.11	2.51	3.62	1.11	2.37	−2.37	1.26	2.23
2	native (ER)	−3.55	−0.07	3.48	3.55	0.07	1.81	−1.81	1.74	0.94
3	BCIPP	−5.29	−5.05	0.24	5.29	5.05	5.17	−5.17	0.12	111.37
4	BDCIPP	−5.68	−5.37	0.31	5.68	5.37	5.53	−5.53	0.16	98.47
5	DPHP	−4.24	−4.23	0.01	4.24	4.23	4.24	−4.24	0.005	1793.52

$$\mathrm{IP} = -E_H \qquad \mathrm{EA} = -E_L \qquad \chi = \frac{(\mathrm{IP} + \mathrm{EA})}{2}$$

$$\mu = \frac{(E_H + E_L)}{2} \qquad \eta = \frac{(\mathrm{IP} - \mathrm{EA})}{2} \qquad \omega = \frac{\mu^2}{2}\eta$$

[a]All values are given in eV.

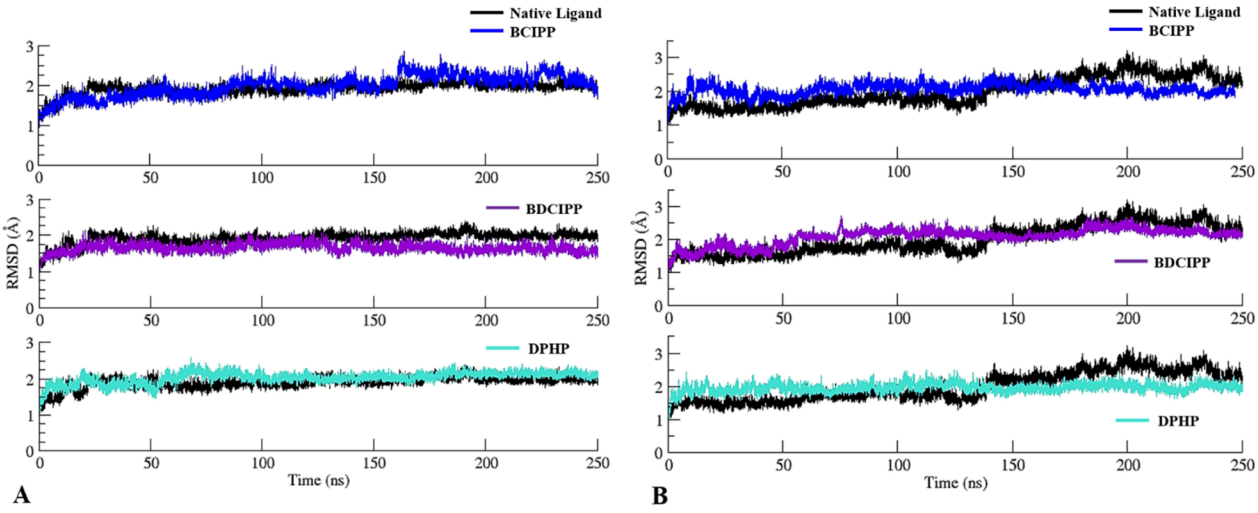

Figure 5. RMSD plots of the 250 ns simulated trajectories of (A) MR and (B) ER with the OPFR metabolites BCIPP, BDCIPP, and DPHP and the native ligand.

contours are situated around oxygen and hydrogen atoms, indicating nucleophilic and electrophilic sites, respectively. Moreover, dark greenish contours around the phenolic part of 4J26 can be observed, which shows a weak nucleophilic site. BCIPP and BDCIPP exhibit strong and weak nucleophilic attack sites at the phosphate and chloropropane moieties, respectively. The predicted favorable electrophilic and nucleophilic attack sites in the DPHP molecule are located around oxygen atoms of the phosphate moiety and arylic hydrogen. These nucleophilic and electrophilic attack sites can be implicated in potential hydrogen binding with the target receptors.

3.4. Frontier Molecular Orbital Analysis. The inter/intramolecular charge transfer areas and a molecule's chemical reactivity can only be ascertained by looking at the frontier molecular orbitals' spatial distribution. Figure 4 shows the isosurfaces of the ligands under study for the highest occupied molecular orbital (HOMO) and lowest unoccupied molecular orbital (LUMO). The red and blue isosurfaces represent negatively and positively charged regions. It can be observed that MR and ER have larger energy gaps (E_g) of 2.51 and 3.48 eV, respectively, predicting that these molecules are kinetically more stable. The isosurfaces of HOMO and LUMO in the MR and ER are situated on the same side of the molecule, showing poor intramolecular charge transfer in these molecules. However, the energy gaps obtained for BCIPP, BDCIPP, and DPHP are comparatively smaller than those of the MR and ER, indicating that these compounds are more polarizable with high chemical and biological reactivity. DPHP can be considered a highly reactive ligand with a band gap of 0.01 eV. Furthermore, the HOMO and LUMO of these compounds encompass the whole molecular structure, showing better charge transport performance of these compounds.

3.5. Reactivity Descriptors. The quantitative measures known as reactivity indices offer crucial information about a molecule's stability or reactivity. Table 2 lists a number of significant reactivity descriptors calculated with equations taken from previous studies,[41,42] such as the electrophilicity index (ω), chemical potential (μ), electron affinity (EA), electronegativity (χ), and ionization potential (IP). The native ligands of MR and ER exhibit relatively smaller values of IP, EA, χ, μ, and ω with ER showing the least values. However, they show larger values of energy gap and chemical hardness as compared to OPFR metabolites, indicating low chemical reactivity and high stability of these molecules. All the OPFR metabolite ligands (BCIPP, BDCIPP, and DPHP) demonstrate larger values of electronegativities and chemical potential, indicating strong intramolecular attraction and hence efficient charge transfer. The chemical hardness of the OPFR metabolite ligands increases in the following order: DPHP (0.005 eV) < BCIPP (0.12 eV) < BDCIPP (0.16 eV), which shows DPHP to be highly reactive in a certain chemical or biological environment. In addition, DPHP also possesses a high electrophilicity index value due to which it may have a high tendency to attract electrons from its surroundings. The reactivity of OPFR metabolite ligands increases as BDCIPP <

https://doi.org/10.1021/acsomega.5c02044
ACS Omega 2025, 10, 20015−20025

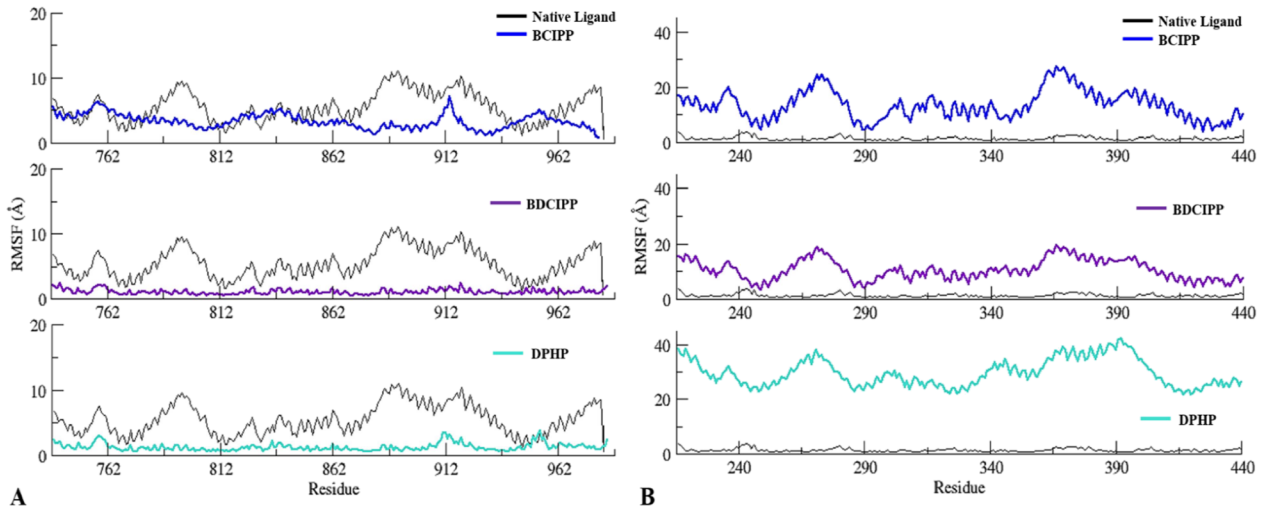

Figure 6. RMSF plots of the 250 ns simulated trajectories of (A) MR and (B) ER with the OPFR metabolites BCIPP, BDCIPP, and DPHP and the native ligand.

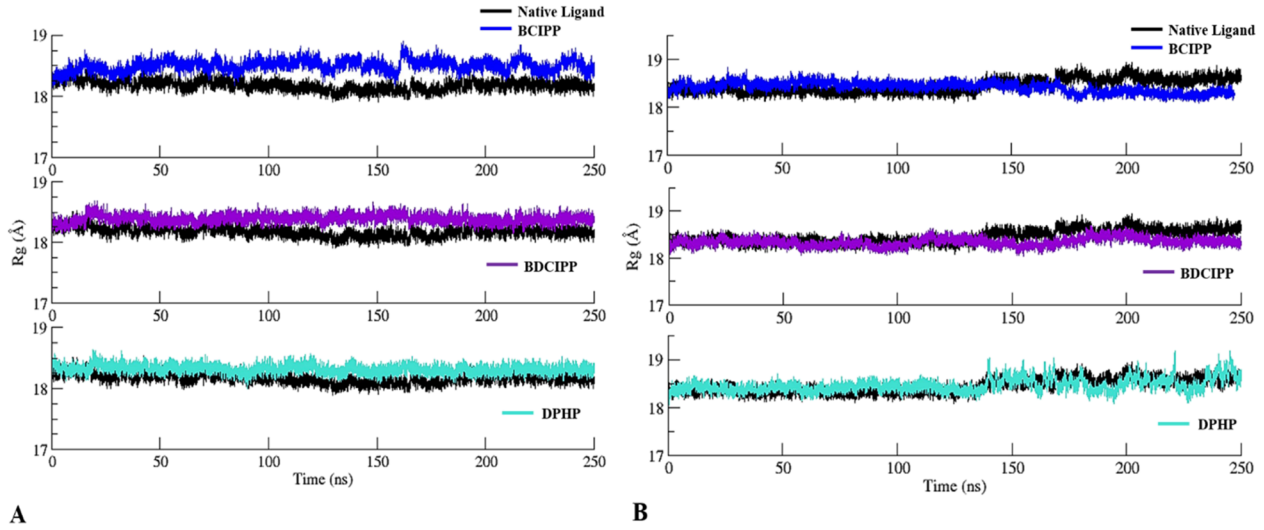

Figure 7. R_g plots of the 250 ns simulated trajectories of (A) MR and (B) ER with OPFR metabolites BCIPP, BDCIPP, DPHP, and the native ligand.

BCIPP < DPHP, and all OPFR metabolite ligands are good electrophiles and exhibit superior charge transport characteristics.

3.6. Assessment of the Structural Stability. The RMSD is a quantitative measure that is used to evaluate the deviation between a protein's native and final conformations during MD simulations, providing valuable insights into the protein's stability and dynamic behavior. In structural biology, RMSD is an essential parameter for evaluating the stability of simulated biomolecular systems, where generally, lower values signify greater stability and higher values indicate less stable complexes.

The RMSDs of the 250 ns simulated trajectories of each complex were computed in order to assess the stability of the structure and fundamental dynamics of MR and ER complexed with the OPFR metabolites. As can be observed in Figure 5A,B, in the case of both MR and ER, consistent RMSDs with few fluctuations were observed for the entire length of the simulation. MR demonstrated an average RMSD of 1.98 ± 0.26, 1.63 ± 0.12, 2.02 ± 0.15, and 1.90 ± 0.15 Å, while ER exhibited an average of 2.04 ± 0.16, 2.08 ± 0.25, 1.95 ± 0.13, and 1.98 ± 0.43 Å in complex with BCIPP, BDCIPP, DPHP, and the native ligand, respectively. All of the systems demonstrated an approximate projected deviation value of around 2 Å, comparable with the native complex, suggesting stable complexes. RMSDs of the 250 ns simulated trajectories of the three complexes along with the native complex are also presented overlapped with each other in Supplementary Figure S1 for the ease of comparison.

3.7. Analysis of Structural Flexibility. To evaluate the MR and ER residues' intrinsic flexibility over the full MD simulation, RMSFs of the 250 ns simulated trajectories were calculated. Higher values within a biomolecular system indicate flexibility and a less stable state. RMSF gives information regarding residue-level disturbances. Conversely, a lower fluctuation level gives the system more stability.

As can be observed in Figure 6A, in the case of MR, all three complexes showed minimal fluctuations, depicting greater stability compared with the native ligand, suggesting competitive binding of the OPFR metabolites with MR, which might be due to the highly reactive species such as the phosphate moieties attached with the OPFR metabolites, also

https://doi.org/10.1021/acsomega.5c02044
ACS Omega 2025, 10, 20015−20025

Table 3. Binding Free Energy (ΔG_{bind}) of the Protein−Ligand Complexes and the Contributions of Various Energetic Terms to the Overall ΔG_{bind}[a]

systems	ΔG_{vdW}	ΔG_{ele}	ΔG_{solv}^{ele}	$\Delta G_{solv}^{nonpolar}$	ΔG_{bind}
MR-BCIPP	−28.98 ± 0.05	−94.89 ± 0.23	117.53 ± 0.19	−3.96 ± 0.01	−10.31 ± 0.07
MR-BDCIPP	−33.38 ± 0.06	−95.14 ± 0.21	120.04 ± 0.19	−4.22 ± 0.01	−12.71 ± 0.08
MR-DPHP	−3.79 ± 0.13	−44.28 ± 1.33	47.67 ± 1.37	−0.55 ± 0.02	−0.96 ± 0.06
MR-native	−50.62 ± 0.07	−14.29 ± 0.08	24.31 ± 0.06	−6.37 ± 0.01	−46.97 ± 0.07
ER-BCIPP	−31.22 ± 0.06	−127.78 ± 0.24	150.09 ± 0.24	−4.05 ± 0.01	−12.95 ± 0.63
ER-BDCIPP	−35.06 ± 0.06	−124.22 ± 0.22	145.36 ± 0.20	−4.58 ± 0.01	−18.49 ± 0.08
ER-DPHP	−3.96 ± 0.14	−73.26 ± 1.36	76.28 ± 1.44	−0.57 ± 0.02	−1.51 ± 0.08
ER-native	−42.49 ± 0.07	−19.03 ± 0.18	25.06 ± 0.12	−5.43 ± 0.01	−41.89 ± 0.07

[a]The results are provided as the mean ± standard error of the mean. All the values provided are in units of kcal/mol.

allowing the formation of additional hydrogen bonds, stabilizing the interaction with the protein residues. The average RMSF values were noted as 3.28 ± 1.12, 1.04 ± 0.37, 1.24 ± 0.57, and 5.68 ± 3.35 Å with BCIPP, BDCIPP, DPHP, and the native ligand, respectively.

In the case of ER, as can be observed in Figure 6B, high fluctuations were recorded in all three complexes when compared with the native ligand, suggesting that the binding of the OPFR metabolites disrupted the protein residues. The average RMSF values were noted as 13.50 ± 5.4, 10.46 ± 3.64, 29.4 ± 5.3, and 2.43 ± 5.7 Å with BCIPP, BDCIPP, DPHP, and the native ligand, respectively. The observed difference in the RMSF values between the OPFR metabolites and native ligand can be explained by the absence of any hydrogen bonding with the ER residues, causing the protein to undergo conformational changes in order to accommodate the ligand, thereby resulting in high flexibility and fluctuations. RMSFs of the 250 ns simulated trajectories of the three complexes, along with the native complex, are also presented overlapped with each other in Figure S2 for the ease of comparison.

3.8. Evaluation of Structural Compactness. Further study was carried out on the time-dependent convergence of the radius of gyration (R_g), which describes the structural characteristics of the simulated ensembles. The results are shown in Figure 7. The root-mean-squared distance between the protein's constituent parts and its center of mass is known as R_g, and it indicates how compact the protein is. After evaluating the molecular effects of ligand binding on the receptor, we used R_g to investigate the folding dynamics of the protein across time. R_g values fluctuate over time in an improperly folded conformation, but stable gyration values are usually maintained by a properly folded conformation.

As can be observed in Figure 7A,B, both MR and ER displayed minimal fluctuations in complex with BCIPP, BDCIPP, and DPHP when compared with the native ligand, displaying average values of 18.49 ± 0.09, 18.39 ± 0.06, 18.31 ± 0.06, and 18.17 ± 0.07 Å and 18.41 ± 0.10, 18.33 ± 0.08, 18.46 ± 0.13, and 18.45 ± 0.14 Å, respectively, suggesting structural compactness rendering stability to the protein complex. Rg plots of the 250 ns simulated trajectories of the three complexes, along with the native complex, are also presented overlapped with each other in Supplementary Figure S3 for the ease of comparison.

3.9. Evaluation of Binding Affinity. The determination of binding free energies (ΔG_{bind}) is an essential step in structure-based drug design for understanding the interaction between a ligand and a protein. In this study, ΔG_{bind} has been calculated for all the protein−ligand complexes using the MM-GBSA equation to provide a more comprehensive understanding of the interaction network that influences the formation of the complex. A higher negative value of ΔG_{bind} indicates a stronger affinity between the ligand and receptor, whereas a lower negative value suggests a lower affinity and therefore less persistent binding. Table 3 presents the computed free energies for the studied OPFR metabolites. The results show that the primary factor favoring the binding process is the ability of the compounds to form van der Waals and electrostatic interactions with the target proteins. BDCIPP showed the highest ΔG_{bind} followed by BCIPP with both MR and ER featuring the values of −12.71, −10.1, and −18.49, −12.95 kcal/mol, respectively, while DPHP did not show favorable binding affinity with both the receptors. A detailed analysis of the individual energy components contributing to the binding process was also conducted. The decomposition of total energy revealed that the nonelectrostatic interactions, such as van der Waals (E_{vdw}) and electrostatic interactions (E_{ele}), were primarily favorable. However, the polar components were found to be unfavorable for binding across the tested OPFR metabolites. This comprehensive binding energy analysis suggests stable and favorable energetic mechanisms driving the molecular recognition between the OPFR metabolites and the target receptors.

3.10. Conformational Motions and the Thermodynamic Landscape. A side by side representation of the PCA and FEL profiles for both proteins, illustrated in Figure 8 (MR) and Figure 9 (ER), highlights their stability, with minimal changes observed when interacting with the investigated ligands.

The MD trajectory of the protein with its native ligand (Figure 8A) maintains a stable conformation. The PC1 and PC2 values in the PCA plot mostly remain within the 5 to −5 range, indicating minimal variability and deviation from the main conformation. The FEL further confirms this with a single, large, stable free energy basin. Similarly, Figure 8B−D reveal that the protein shows minimal instability when interacting with the OPFR metabolites. The PCA plots consistently depict the protein maintaining a stable conformation with little variation, as PC1 and PC2 values remain within the 5 to −5 range for most of the trajectory. The FELs for the investigated ligands also exhibit minimal alterations to the single stable basin contour seen in the FEL plot with the native ligand.

Similarly, the PCA plots and FEL of protein ER, as shown in Figure 9, indicate that it is also highly stable with minimal variability and large free energy basins when interacting with both the native ligand and OPFR metabolites. The PCA reveals an MD trajectory where the protein consistently maintains a stable conformation with little variation. The FEL

https://doi.org/10.1021/acsomega.5c02044
ACS Omega 2025, 10, 20015−20025

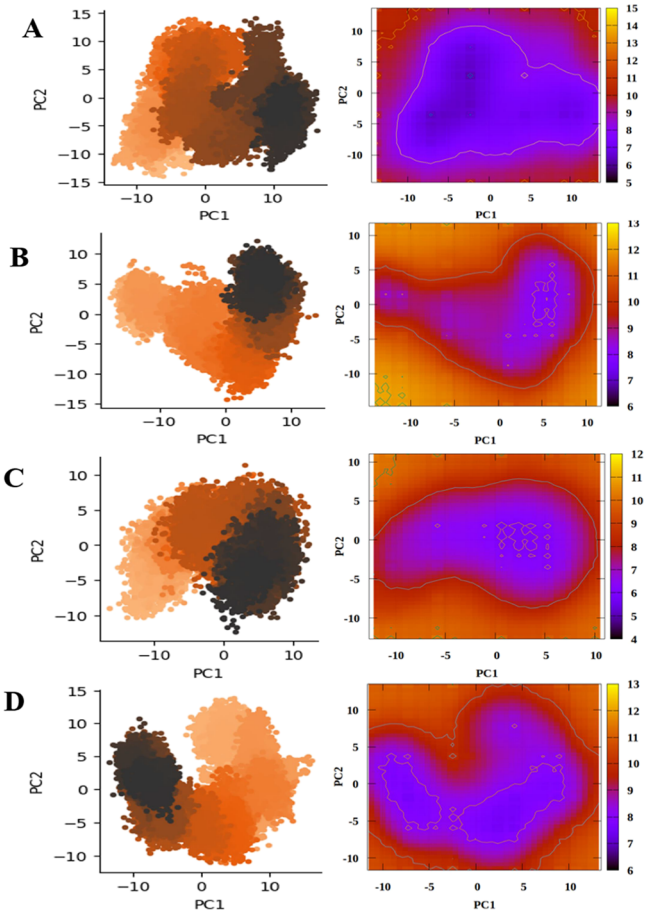

Figure 8. Side by side representation of the PCA and Free Energy Landscape (FEL) profiles of MR in complex with (A) Native, (B) BCIPP, (C) BDCIPP, and (D) DPHP.

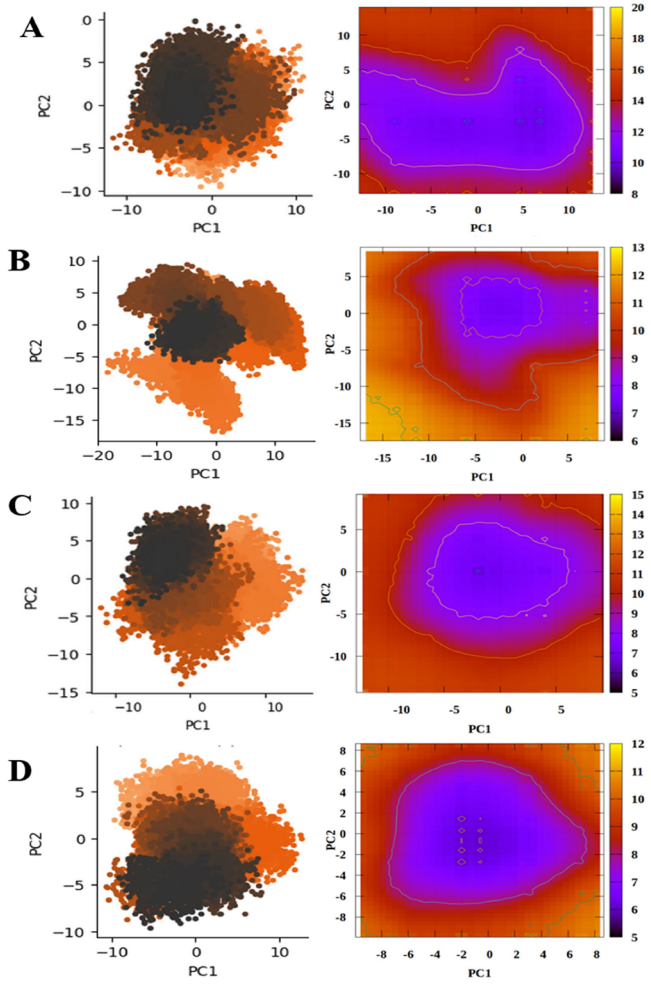

Figure 9. Side by side representation of the PCA and Free Energy Landscape (FEL) profiles of ER in complex with (A) Native, (B) BCIPP, (C) BDCIPP, and (D) DPHP.

of the protein with the native ligand displays a very large free energy basin, which remains largely unchanged by the presence of the OPFR metabolites, as depicted in Figure 9B–D. This demonstrates that both MR and ER retain their structural integrity and stability in the presence of the OPFR metabolites, comparable to that of the native ligand. This stability is crucial as it suggests that the proteins maintain their functional conformations while interacting with the ligands under investigation.

4. CONCLUSIONS

This study employed a comprehensive computational approach, integrating molecular docking, density functional theory, and all-atom MD simulations, to explore the binding interactions of the key OPFR metabolites BCIPP, BDCIPP, and DPHP with human ER and MR. The findings revealed that these metabolites formed stable and compact complexes with both MR and ER, though higher-residue atomic fluctuations were observed in ER complexes, suggesting a disruption of the normal protein function. Binding free energy analysis further supported favorable interactions between the metabolites and target receptors. Additionally, PCA, aided by machine learning algorithms, indicated consistent molecular motion, while free energy profiles revealed stable energy basins with minimal variation. These findings highlight the strong binding affinities of OPFR metabolites with both the MR and ER, suggesting their potential to act as endocrine disruptors at the molecular level. In conclusion, this study provides valuable insights into the MD underlying binding of OPFR metabolites with the ER and MR, laying the foundation for further investigations into their environmental and health hazards.

■ ASSOCIATED CONTENT

Supporting Information

The Supporting Information is available free of charge at https://pubs.acs.org/doi/10.1021/acsomega.5c02044.

RMSD plots of the 250 ns simulated trajectories of MR and ER with the OPFR metabolites BCIPP, BDCIPP, DPHP, and the reference ligand; RMSF plots of the 250 ns simulated trajectories of MR and ER with the OPFR metabolites BCIPP, BDCIPP, DPHP, and the reference ligand; R_g plots of the 250 ns simulated trajectories of MR and ER with the OPFR metabolites BCIPP, BDCIPP, DPHP, and the reference ligand; and superimposed poses of MR with OPFR metabolites BCIPP, BDCIPP, DPHP, and the reference ligand (PDF)

■ AUTHOR INFORMATION

Corresponding Author

Zaheer Ul-Haq − *Dr. Panjwani Center for Molecular Medicine and Drug Research, International Center for Chemical and*

https://doi.org/10.1021/acsomega.5c02044
ACS Omega 2025, 10, 20015−20025

Biological Sciences, University of Karachi, Karachi 75270, Pakistan; orcid.org/0000-0002-8530-8711; Email: zaheer.qasmi@iccs.edu

Authors

Syeda Sumayya Tariq − *Dr. Panjwani Center for Molecular Medicine and Drug Research, International Center for Chemical and Biological Sciences, University of Karachi, Karachi 75270, Pakistan;* orcid.org/0000-0001-5692-8703

Madiha Sardar − *H.E.J. Research Institute of Chemistry, International Center for Chemical and Biological Sciences, University of Karachi, Karachi 75270, Pakistan*

Muhammad Shafiq − *H.E.J. Research Institute of Chemistry, International Center for Chemical and Biological Sciences, University of Karachi, Karachi 75270, Pakistan;* orcid.org/0009-0007-8370-9056

Muhammad Huzaifa − *H.E.J. Research Institute of Chemistry, International Center for Chemical and Biological Sciences, University of Karachi, Karachi 75270, Pakistan*

Mohammad Nur-e-Alam − *Department of Pharmacognosy, College of Pharmacy, King Saud University, Riyadh 11451, Kingdom of Saudi Arabia*

Yan Wang − *State Key Laboratory for Chemistry and Molecular Engineering of Medicinal Resources, Key Laboratory for Chemistry and Molecular Engineering of Medicinal Resources (Ministry of Education of China), Guilin 541004, China; Key Laboratory for Chemistry and Molecular Engineering of Medicinal Resources, School of Chemistry and Pharmaceutical Sciences, Guangxi Normal University, Guilin 541004, China;* orcid.org/0000-0001-9786-7492

Complete contact information is available at: https://pubs.acs.org/10.1021/acsomega.5c02044

Author Contributions

#S.S.T. and M.S. have contributed equally.

Notes

The authors declare no competing financial interest.

■ ACKNOWLEDGMENTS

The authors extend their appreciation to the Researchers Supporting Project number (RSPD2025R994), King Saud University, Riyadh, Saudi Arabia.

■ REFERENCES

(1) Hoffman, K.; Daniels, J. L.; Stapleton, H. M. Urinary metabolites of organophosphate flame retardants and their variability in pregnant women. *Environ. Int.* **2014**, *63*, 169−172.

(2) Marklund, A.; Andersson, B.; Haglund, P. Screening of organophosphorus compounds and their distribution in various indoor environments. *Chemosphere* **2003**, *53* (9), 1137−1146.

(3) Stapleton, H. M.; Klosterhaus, S.; Keller, A.; Ferguson, P. L.; Van Bergen, S.; Cooper, E.; Webster, T. F.; Blum, A. Identification of flame retardants in polyurethane foam collected from baby products. *Environ. Sci. Technol.* **2011**, *45* (12), 5323−5331.

(4) Kajiwara, N.; Noma, Y.; Takigami, H. Brominated and organophosphate flame retardants in selected consumer products on the Japanese market in 2008. *Journal of hazardous materials* **2011**, *192* (3), 1250−1259.

(5) Beyer, G. Introduction to flame retardant systems. In *Flame Retardant Nanocomposites*; Elsevier, 2024; pp 1−22.

(6) Blum, A.; Behl, M.; Birnbaum, L. S.; Diamond, M. L.; Phillips, A.; Singla, V.; Sipes, N. S.; Stapleton, H. M.; Venier, M. Organophosphate ester flame retardants: are they a regrettable substitution for polybrominated diphenyl ethers? *Environmental science & technology letters* **2019**, *6* (11), 638−649.

(7) Serreau, R.; Terbeche, Y.; Rigourd, V. *Pollutants in Breast Milk: A Scoping Review of the Most Recent Data in 2024*; Healthcare, MDPI, 2024; p 680.

(8) Chupeau, Z.; Bonvallot, N.; Mercier, F.; Le Bot, B.; Chevrier, C.; Glorennec, P. Organophosphorus flame retardants: a global review of indoor contamination and human exposure in Europe and epidemiological evidence. *International journal of environmental research and public health* **2020**, *17* (18), 6713.

(9) Hou, M.; Shi, Y.; Na, G.; Cai, Y. A review of organophosphate esters in indoor dust, air, hand wipes and silicone wristbands: Implications for human exposure. *Environ. Int.* **2021**, *146*, No. 106261.

(10) Cooper, E.; Covaci, A.; Van Nuijs, A.; Webster, T.; Stapleton, H. Analysis of the flame retardant metabolites bis (1, 3-dichloro-2-propyl) phosphate (BDCPP) and diphenyl phosphate (DPP) in urine using liquid chromatography−tandem mass spectrometry. *Anal. Bioanal. Chem.* **2011**, *401*, 2123−2132.

(11) Butt, C. M.; Congleton, J.; Hoffman, K.; Fang, M.; Stapleton, H. M. Metabolites of organophosphate flame retardants and 2-ethylhexyl tetrabromobenzoate in urine from paired mothers and toddlers. *Environ. Sci. Technol.* **2014**, *48* (17), 10432−10438.

(12) Dishaw, L. V.; Macaulay, L. J.; Roberts, S. C.; Stapleton, H. M. Exposures, mechanisms, and impacts of endocrine-active flame retardants. *Curr. Opin. Pharmacol.* **2014**, *19*, 125−133.

(13) Wang, X.; Hales, B. F.; Robaire, B. Effects of flame retardants on ovarian function. *Reproductive Toxicology* **2021**, *102*, 10−23.

(14) Zhang, Q.; Yu, C.; Fu, L.; Gu, S.; Wang, C. New insights in the endocrine disrupting effects of three primary metabolites of organophosphate flame retardants. *Environ. Sci. Technol.* **2020**, *54* (7), 4465−4474.

(15) Liu, X.; Ji, K.; Choi, K. Endocrine disruption potentials of organophosphate flame retardants and related mechanisms in H295R and MVLN cell lines and in zebrafish. *Aquatic toxicology* **2012**, *114*, 173−181.

(16) Beachy, M. D.; Chasman, D.; Murphy, R. B.; Halgren, T. A.; Friesner, R. A. Accurate ab initio quantum chemical determination of the relative energetics of peptide conformations and assessment of empirical force fields. *J. Am. Chem. Soc.* **1997**, *119* (25), 5908−5920.

(17) Halgren, T. A. Merck molecular force field. I. Basis, form, scope, parameterization, and performance of MMFF94. *J. Comput. Chem.* **1996**, *17* (5−6), 490−519.

(18) Fuller, P. J.; Yao, Y.-Z.; Yang, J.; Young, M. J. Structural determinants of activation of the mineralocorticoid receptor: an evolutionary perspective. *Journal of Human Hypertension* **2021**, *35* (2), 110−116.

(19) Fuchs, S.; Nguyen, H. D.; Phan, T. T. P.; Burton, M. F.; Nieto, L.; de Vries-van Leeuwen, I. J.; Schmidt, A.; Goodarzifard, M.; Agten, S. M.; Rose, R.; Ottmann, C.; Milroy, L. G.; Brunsveld, L. Proline primed helix length as a modulator of the nuclear receptor−coactivator interaction. *J. Am. Chem. Soc.* **2013**, *135* (11), 4364−4371.

(20) Labute, P. *Protonate 3D: assignment of macromolecular protonation state and geometry*; Chemical Computing Group Inc., 2007.

(21) Labute, P. The generalized Born/volume integral implicit solvent model: estimation of the free energy of hydration using London dispersion instead of atomic surface area. *J. Comput. Chem.* **2008**, *29* (10), 1693−1698.

(22) Kühne, T. D.; Iannuzzi, M.; Del Ben, M.; Rybkin, V. V.; Seewald, P.; Stein, F.; Laino, T.; Khaliullin, R. Z.; Schütt, O.; Schiffmann, F.; Golze, D.; Wilhelm, J. CP2K: An electronic structure and molecular dynamics software package-Quickstep: Efficient and accurate electronic structure calculations. *J. Chem. Phys.* **2020**, *152* (19), 194103.

(23) Krishnan, R.; Binkley, J. S.; Seeger, R.; Pople, J. A. Self-consistent molecular orbital methods. XX. A basis set for correlated wave functions. *J. Chem. Phys.* **1980**, *72* (1), 650−654.

(24) Becke, A. D. Density-functional exchange-energy approximation with correct asymptotic behavior. *Phys. Rev. A* **1988**, *38* (6), 3098.
(25) Lee, C.; Yang, W.; Parr, R. G. Development of the Colle-Salvetti correlation-energy formula into a functional of the electron density. *Phys. Rev. B* **1988**, *37* (2), 785.
(26) Case, D. A.; Cheatham, T. E., III; Darden, T.; Gohlke, H.; Luo, R.; Merz, K. M., Jr; Onufriev, A.; Simmerling, C.; Wang, B.; Woods, R. J. The Amber biomolecular simulation programs. *J. Comput. Chem.* **2005**, *26* (16), 1668−1688.
(27) Wang, J.; Wang, W.; Kollman, P. A.; Case, D. A. Antechamber: an accessory software package for molecular mechanical calculations. *J. Am. Chem. Soc.* **2001**, *222* (1), 2001.
(28) Mark, P.; Nilsson, L. Structure and dynamics of the TIP3P, SPC, and SPC/E water models at 298 K. *J. Phys. Chem. A* **2001**, *105* (43), 9954−9960.
(29) Fletcher, R.; Powell, M. J. A rapidly convergent descent method for minimization. *computer journal* **1963**, *6* (2), 163−168.
(30) Darden, T.; York, D.; Pedersen, L. Particle mesh Ewald: An N· log (N) method for Ewald sums in large systems. *J. Chem. Phys.* **1993**, *98* (12), 10089−10092.
(31) Kräutler, V.; Van Gunsteren, W. F.; Hünenberger, P. H. A fast SHAKE algorithm to solve distance constraint equations for small molecules in molecular dynamics simulations. *J. Comput. Chem.* **2001**, *22* (5), 501−508.
(32) Pettersen, E. F.; Goddard, T. D.; Huang, C. C.; Couch, G. S.; Greenblatt, D. M.; Meng, E. C.; Ferrin, T. E. UCSF Chimera—a visualization system for exploratory research and analysis. *J. Comput. Chem.* **2004**, *25* (13), 1605−1612.
(33) Humphrey, W.; Dalke, A.; Schulten, K. VMD: visual molecular dynamics. *J. Mol. Graphics* **1996**, *14* (1), 33−38.
(34) Roe, D. R.; Cheatham, T. E., III PTRAJ and CPPTRAJ: software for processing and analysis of molecular dynamics trajectory data. *J. Chem. Theory Comput.* **2013**, *9* (7), 3084−3095.
(35) Miller, B. R., III; McGee, T. D., Jr; Swails, J. M.; Homeyer, N.; Gohlke, H.; Roitberg, A. E. MMPBSA. py: an efficient program for end-state free energy calculations. *J. Chem. Theory Comput.* **2012**, *8* (9), 3314−3321.
(36) Genheden, S.; Ryde, U. The MM/PBSA and MM/GBSA methods to estimate ligand-binding affinities. *Expert opinion on drug discovery* **2015**, *10* (5), 449−461.
(37) Patodia, S.; Bagaria, A.; Chopra, D. Molecular dynamics simulation of proteins: a brief overview. *J. Phys. Chem. Biophys.* **2014**, *4* (6), 166.
(38) Singh, A. K.; Kushwaha, P. P.; Prajapati, K. S.; Shuaib, M.; Gupta, S.; Kumar, S. Identification of FDA approved drugs and nucleoside analogues as potential SARS-CoV-2 A1pp domain inhibitor: An in silico study. *Computers in Biology and Medicine* **2021**, *130*, No. 104185.
(39) Chattaraj, K. G.; Paul, S. Underlying Mechanisms of Allopurinol in Eliminating Renal Toxicity Induced by Melamine−Uric Acid Complex Formation: A Computational Study. *Chem. Res. Toxicol.* **2021**, *34* (9), 2054−2069.
(40) Chattaraj, K. G.; Paul, S. Appraising the potency of small molecule inhibitors and their graphene surface-mediated organizational attributes on uric acid−melamine clusters. *Phys. Chem. Chem. Phys.* **2022**, *24* (2), 1029−1047.
(41) Parr, R. G.; Donnelly, R. A.; Levy, M.; Palke, W. E. Electronegativity: the density functional viewpoint. *J. Chem. Phys.* **1978**, *68* (8), 3801−3807.
(42) Parr, R. G.; Szentpály, L. v.; Liu, S. Electrophilicity index. *J. Am. Chem. Soc.* **1999**, *121* (9), 1922−1924.

https://doi.org/10.1021/acsomega.5c02044
ACS Omega 2025, 10, 20015−20025